RSC Advances

PAPER

View Article Online
View Journal | View Issue

Cite this: *RSC Adv.*, 2020, **10**, 29975

A stable TiO_2–graphene nanocomposite anode with high rate capability for lithium-ion batteries†

Umer Farooq,[a] Faheem Ahmed,[b] Syed Atif Pervez,[c] Sarish Rehman,[d] Michael A. Pope,[d] Maximilian Fichtner[c] and Edward P. L. Roberts*[a]

Received 16th June 2020
Accepted 28th July 2020

DOI: 10.1039/d0ra05300g

rsc.li/rsc-advances

A rapid microwave hydrothermal process is adopted for the synthesis of titanium dioxide and reduced graphene oxide nanocomposites as high-performance anode materials for Li-ion batteries. With the assistance of hydrazine hydrate as a reducing agent, graphene oxide was reduced while TiO_2 nanoparticles were grown *in situ* on the nanosheets to obtain the nanocomposite material. The morphology of the nanocomposite obtained consisted of TiO_2 particles with a size of ~100 nm, uniformly distributed on the reduced graphene oxide nanosheets. The as-prepared TiO_2–graphene nanocomposite was able to deliver a capacity of 250 mA h g^{-1} ± 5% at 0.2C for more than 200 cycles with remarkably stable cycle life during the Li^+ insertion/extraction process. In terms of high rate capability performance, the nanocomposite delivered discharge capacity of *ca.* 100 mA h g^{-1} with >99% coulombic efficiency at C-rates of up to 20C. The enhanced electrochemical performance of the material in terms of high rate capability and cycling stability indicates that the as-developed TiO_2–rGO nanocomposites are promising electrode materials for future Li-ion batteries.

Introduction

Li-ion batteries (LIBs) are considered to be the most attractive electrochemical energy storage technology among all technologies for portable devices and electric vehicles.[1] With growing interest in developing green electrode materials for future LIBs, attention has also been given to TiO_2 as a negative electrode material.[2–4] TiO_2 can be a viable electrode material because of its stable cycle life, low environmental impact, low cost, and abundance.[5,6] The relatively higher working voltage of a TiO_2 anode (≥1.5 V *vs.* Li^+/Li) compromises the overall energy density of the cell but it can also effectively slows the growth of irreversible formation of an SEI layer, which consequently improves the coulombic efficiency compared to conventional carbon-based anode materials.[7] However, the major challenge in its practical application for the anode in LIBs is its low electronic conductivity of TiO_2 (~10^{-12} S cm^{-1})[8] which limits the rate capability and LIB performance.

To enhance the rate capability, extensive efforts have been deployed to increase the surface area of active material. Thus, the mobility of electrons and Li ions is facilitated by decreasing the diffusion path and controlling the stress mechanism. This was achieved by developing TiO_2 nanotubes, nanowires, and altering the crystal structures of material through high temperature calcination.[9–18] However, as discussed above the low electrical conductivity of TiO_2 still limits its electrochemical performance for battery application.[19] TiO_2 composites with carbon and metal oxides have demonstrated improvements in electronic conductivity, but more work is required to achieve a material which can be of technical relevance.[20–24] Compared to the traditional carbonaceous additives, graphene is considered promising to improve the electrochemical performances of various electrode materials due to its high electrical conductivity, superior mechanical strength and large surface area.[25,26] These properties make graphene a suitable material for use in a TiO_2 composite anode for LIBs.

The conventional methods to synthesize TiO_2 nanostructures include sol–gel methods which can be utilized to develop TiO_2–graphene nanocomposites.[27,28] Nevertheless, these methods often require anhydrous alcohols as solvents and normally yield a mixture of rutile and anatase TiO_2 phases instead of a pure single phase. The rutile TiO_2 phase has been found to exhibit low rate performance when subjected to high current density during cycling.[27] To address this challenge extensive studies such as template-assisted synthesis, electrospinning, and anodization, have been carried out to obtain structures suitable for fast electron and Li^+ mobility.[29–33] In most

[a]*Department of Chemical and Petroleum Engineering, University of Calgary, 2500 University Drive NW, Calgary, AB, T2N 1N4, Canada. E-mail: edward.roberts@ucalgary.ca*

[b]*Department of Physics, College of Science, King Faisal University, Hofuf, Al-Hassa, Saudi Arabia*

[c]*Helmholtz Institute Ulm (HIU) Electrochemical Energy Storage, Helmholtzstrasse 11, Ulm, 89081, Germany*

[d]*Department of Chemical Engineering, University of Waterloo, 200 University Ave W, Waterloo, ON, T2N 1N4, Canada*

† Electronic supplementary information (ESI) available. See DOI: 10.1039/d0ra05300g

cases an improved battery performance of TiO_2–graphene nanoarchitectures was achieved by altering the synthesis conditions to control the particle size and phase of TiO_2; however, the previously reported methods are time consuming and costly.[6] There is thus a need for a rapid and cost-effective method for developing well-organized TiO_2–graphene nanocomposites for application in LIBs. Herein, we report a swift and scalable method for *in situ* synthesis of TiO_2 nanoparticles on rGO nanosheets *via* a microwave hydrothermal process to obtain a high-performance TiO_2–rGO nanocomposite LIB anode material. These nanocomposites exhibit outstanding rate performance due to the fast mobility of electrons and Li^+ diffusion during insertion/extraction. The improved electrochemical performance demonstrates the viability of this material as a high-rate negative electrode for advanced LIBs.

Experimental

The material synthesis, characterization and electrochemical testing methods used in this study are described below. The synthesis and electrochemical testing methods are also illustrated schematically in Fig. 1.

(a) Synthesis of TiO_2–rGO nanocomposite

GO was synthesized using the Hummers' method[34] for which details are provided in ESI.† The resulting GO obtained was dried at 80 °C after washing with water several times. In the next step, to synthesize the desired TiO_2–rGO nanocomposite, an aqueous solution containing 4 M of titanium(III) chloride precursor and 0.1 M of potassium hydroxide was prepared. Three different concentrations of wt% of rGO (1, 2 and 5) relative to the amount of TiO_2 in the nanocomposite along with 50–100 μl of hydrazine hydrate (HH) reducing agent were added to the solution. The solution was transferred to a hydrothermal microwave (CEM MARS 5) at 160 °C, 160 psi, 900 W for 25 min. After hydrothermal microwave treatment, the product was washed in deionized water and ethanol several times and dried at 80 °C for 15 h. The as-prepared product was ground using a mortar and pestle prior to further study the physical and electrochemical properties. A more detailed description of the synthesis of TiO_2–rGO nanocomposite is presented in the ESI.† Based on the wt% of rGO added to the TiO_2 nanoparticles, these samples are named TiO_2–pristine, TiO_2–rGO 1%, TiO_2–rGO 2%, TiO_2–rGO 5% in the following discussion.

(b) Materials characterization

The structural characterization was performed using a Philips X'Pert MPD 3030 X-ray diffractometer equipped with Cu Kα radiation in the 2θ range of 20–60°. The morphological characterization of the composite was carried out by using field emission scanning electron microscopy (FESEM) and Jeol 2010F transmission electron microscopy (TEM) which was operated at 200 kV. Elemental mapping was obtained using energy-dispersive X-ray spectroscopy (EDS) using the same SEM. The nitrogen adsorption/desorption studies were performed using a Micromeritics ASAP 2020.

(c) Cell fabrication and electrochemical characterization

To explore electrochemical performance of TiO_2–rGO nanocomposite, the working electrode was prepared by using the as-prepared TiO_2–rGO nanocomposites with different amounts of rGO, polyvinylidene difluoride (PVDF) and Super P carbon black with a weight ratio of 8 : 1 : 1, respectively. The active material mass loading in the as-prepared electrodes was in range of 1.9 to 2.5 mg cm^{-2} for different experiments. Once the slurry was prepared, it was coated onto a copper foil and dried overnight. Lithium foil (purity 99.9%) served as the counter electrode, polypropylene (PP) membrane as a separator and 1 M lithium hexaflurophosphate ($LiPF_6$) dissolved in ethylene carbonate (EC) and dimethyl carbonate (DMC) (1 : 1 in vol%) as the electrolyte. The 2032-type coin cells were assembled in an argon filled glovebox with O_2 and H_2O levels less than 0.1 ppm. Galvanostatic cycling and rate capability experiments were performed using multi-channel battery tester (LAND) with

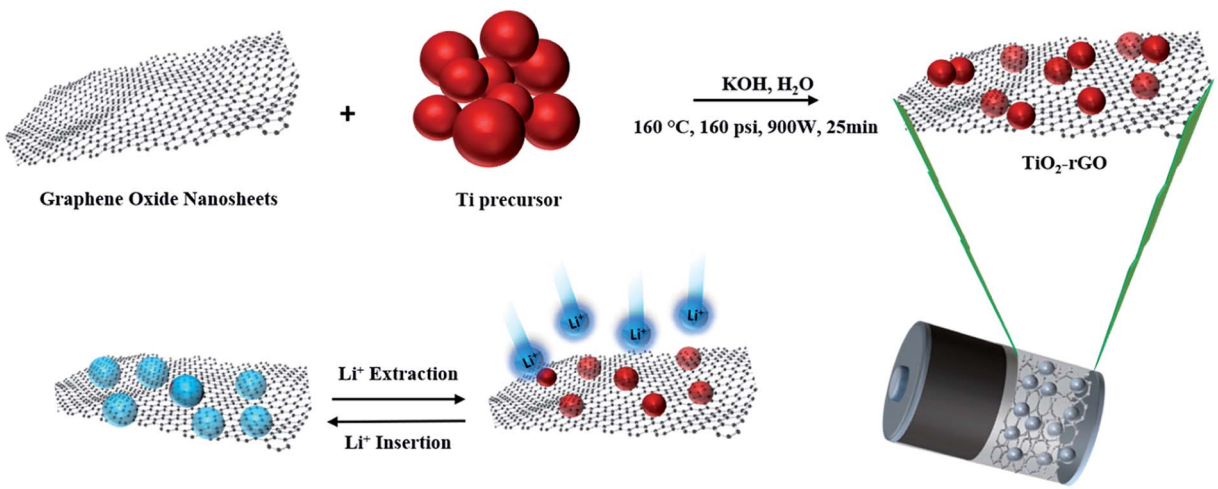

Fig. 1 Schematic illustration of synthesis method of TiO_2–rGO nanocomposite and Li insertion/extraction process.

a potential range between 1 and 2.5 V at a range of current densities. An aging time of 12 h was used before starting the battery cycling. Cyclic voltammetry tests were carried out in a potential range of 0 to 3 V with a scan rate of 0.5 mV s^{-1}. Electrochemical impedance spectroscopy (EIS) tests were conducted in a frequency range of 100 kHz to 10 mHz using a Biologic SP-300 potentiostat.

Results and discussion

The structural and morphological properties of TiO_2-based nanocomposites are strongly dependent on the temperature and time of reaction which consequently affects the electrochemical response of nanocomposite in battery application.[34–36] Although rutile is considered to be most stable TiO_2 phase, it is not favorable for battery anode applications because of the limited Li^+ diffusion along the *c*-axis channels only.[33] It has been reported that anatase phase TiO_2 with <200 nm particle size is thermodynamically stable.[37–39] Thus, it is important to consider both the crystal structure as well as the particle size of TiO_2 in order to achieve better electrochemical performance in LIB negative electrodes.

The synthesis time to obtain the TiO_2–rGO nanocomposite was only around 25 min. The simple process is a convenient synthesis route to prepare the nanocomposite in less time, with the desired morphology and the right crystal structure. Without adding rGO, the synthesized TiO_2 materials (hereinafter referred to as TiO_2–pristine) was found to have an anatase structure, confirmed by XRD analysis (Fig. 2a). The XRD patterns of samples with rGO 1, 2 and 5 wt% revealed that TiO_2 retained this anatase crystalline structure. The anatase phase of the TiO_2 nanoparticles was confirmed by the seven characteristic diffraction peaks (JCPDS 21-1272),[40] while no evidence of rutile phase TiO_2 was observed. The specific surface area and pore size distribution of the sample having maximum rGO content (TiO_2–rGO 5%) was further explored by nitrogen adsorption/desorption studies, and the isotherms obtained are presented in Fig. 2b. The Brunauer–Emmett–Teller (BET) specific surface area of TiO_2–rGO 5% was found to be ~105 m^2 g^{-1}, much higher than that of TiO_2–graphene nanoparticles previously reported.[25,36] The high surface area can be attributed to the uniform distribution and relatively small size of the TiO_2 nanoparticles, as well as the contribution of the graphene sheets in the nanocomposite. The differential pore volume in a plot calculated from the desorption isotherm by BET method (inset graph in Fig. 2b) represents mesopores having an average pore diameter of 7 nm in the nanocomposite. These mesopores in the nanocomposite are expected to be associated with the interparticle space.

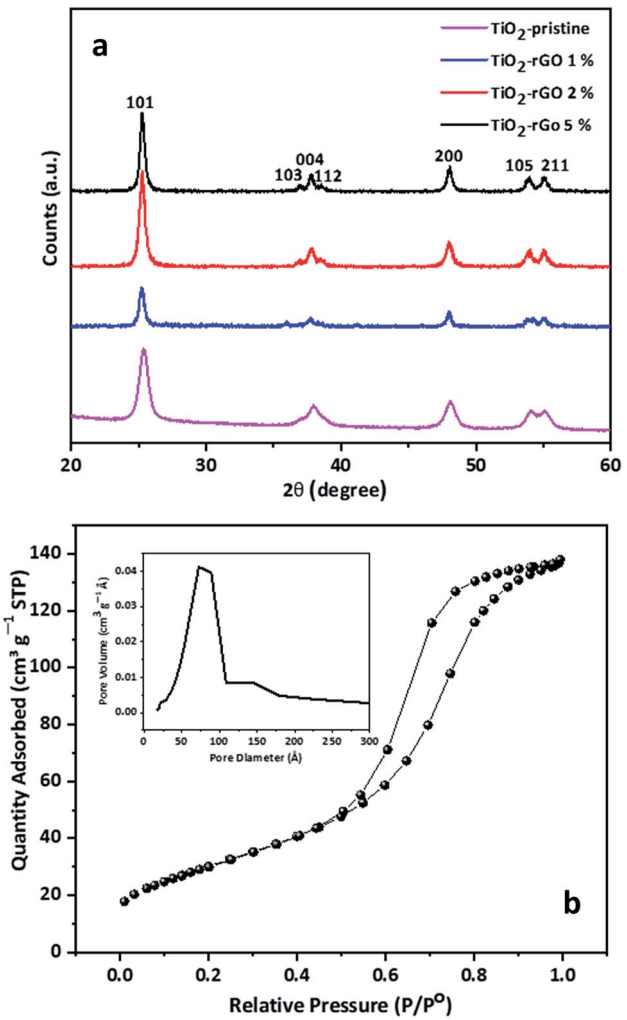

Fig. 2 (a) XRD patterns of TiO_2–pristine, TiO_2–rGO 1%, TiO_2–rGO 2%, TiO_2–rGO 5%. Peaks at 2θ values of 25.3°, 36.9°, 37.8°, 38.5°, 48.0°, 53.8° and 55.0° correspond to the characteristic diffraction peaks of anatase TiO_2 (JCPDS 21-1272).[40] (b) Nitrogen adsorption/desorption isotherms TiO_2–rGO 5%. The inset shows the pore-size distribution plot of the same sample.

The FESEM and TEM. Fig. 3a shows an FESEM image of the TiO_2–rGO 5% sample which reveals well dispersed TiO_2 on GO nanosheets and connected to each other to form a well-defined nanocomposite. The TiO_2 nanoparticles have a size in the range of *ca.* 100 nm. Fig. 3b shows EDS elemental mapping of the area shown in Fig. 3a, which indicates that all the major elements were homogenously present including carbon, titanium and oxygen. Fig. 3c and d present the bright-field TEM images of same sample at two different magnifications. The images confirm the homogenous distribution of TiO_2 particles on sheet. This morphological characterization indicates that the TiO_2 particle size is in the suitable size range for thermodynamic stability (<200 nm (ref. 37–39)), with appropriate pore size to achieve good electrochemical performance in LIBs.

The FESEM image and elemental mapping of TiO_2–rGO 5% is presented in the ESI† along with EDS results Fig. S1 and S2.† Furthermore, the FESEM images of the pristine and samples with different rGO loadings are presented in ESI (Fig. S3).† When the rGO content was increased from 1% to 5%, no visible change was observed in the morphology. Therefore, differences in the electrochemical performance of these materials can be attributed to the rGO to TiO_2 weight ratio rather than differences in the morphological structure, which was found to be independent of the composition ratio.

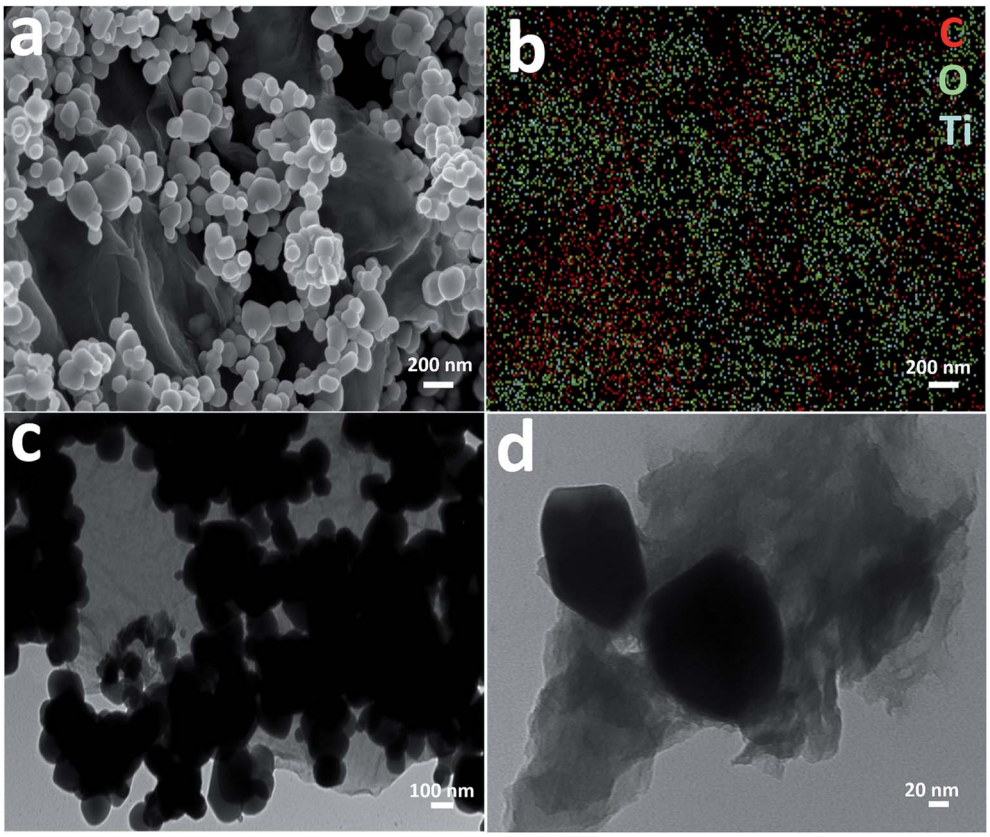

Fig. 3 (a) FESEM image of TiO_2–rGO 5%, (b) EDS elemental mapping of the area shown in (a), (c) bright-field TEM image of TiO_2–rGO 5%, (d) bright-field TEM image at higher magnification.

The electrochemical performance of TiO_2–rGO nanocomposites prepared with 1, 2 and 5 wt% GO as anode materials was evaluated in Li half-cells. A schematic of the coin cell assembly is shown in Fig. S4.† The first galvanostatic discharge/charge voltage profiles of the four samples tested at 0.2C with a voltage window of 1.0–2.5 V are presented in Fig. 4a. With this voltage window no contribution from rGO is anticipated because LiC_6 formation only takes place at potentials lower than 1.0 V. In these samples, all the cells display characteristic discharge and charge voltage plateaus at 1.75 V and 1.85 V, respectively, associated with anatase-TiO_2.[27] The initial discharge and charge capacities of all the three samples were between 125 mA h g^{-1} (based on the mass of the TiO_2–rGO nanocomposite) and 255 mA h g^{-1} with excellent first cycle coulombic efficiencies. These high coulombic efficiencies (>90%) demonstrate that formation of SEI in case of TiO_2 anodes is notably less than for conventional carbon negative electrode materials.[24,41]

The TiO_2–rGO 5% nanocomposite showed the highest first discharge capacity of mA h g^{-1} among all tested samples. The nanocomposite prepared using 2% rGO is comparable to 5%, however, the capacity shown by sample TiO_2–rGO 1% and TiO_2–pristine is significantly lower which is attributed to the low rGO content in the nanocomposite, and thus its relatively low conductivity. Increasing the rGO content from 2 wt% to 5 wt% led to only a small increase in electrochemical performance, suggesting that the percolation threshold of the nanocomposite had been reached and thus the increase in the conductivity was relatively small. Furthermore, 5% graphene content is reported to be the most favorable composition ratio with TiO_2 to achieve best C-rate performance.[26] Adding more than 5% rGO could result in re-stacking of rGO nanosheets, which in turn will limit the diffusion of Li^+. However, further experimental studies could be conducted with higher amounts of rGO to determine the optimum. TiO_2–rGO 5% is expected to have the highest content of rGO and thus will have the highest conductivity. The longest voltage plateau for the TiO_2–rGO 5% confirms that the rGO enhances the discharge capacity. The shorter and similar terminal voltage slope in all the samples show that the capacitive behavior and its contribution in the discharge capacity of these electrodes is negligible.

The TiO_2–rGO 5% shows remarkable cycling stability with superior discharge capacity. The cyclic stability is one of the key features of TiO_2 based anodes which is apparent in the experimental results presented in Fig. 4b. All the cells retained about 90% of their initial capacity after 200 cycles at 0.2C. The average fade in capacity was lower than 1% each cycle while the coulombic efficiency was above 99% for each cycle after first few formation cycles.

The rate capability performance of an anode material is one of the most important parameters for practical application.[30] To evaluate the as-prepared samples for rate capability

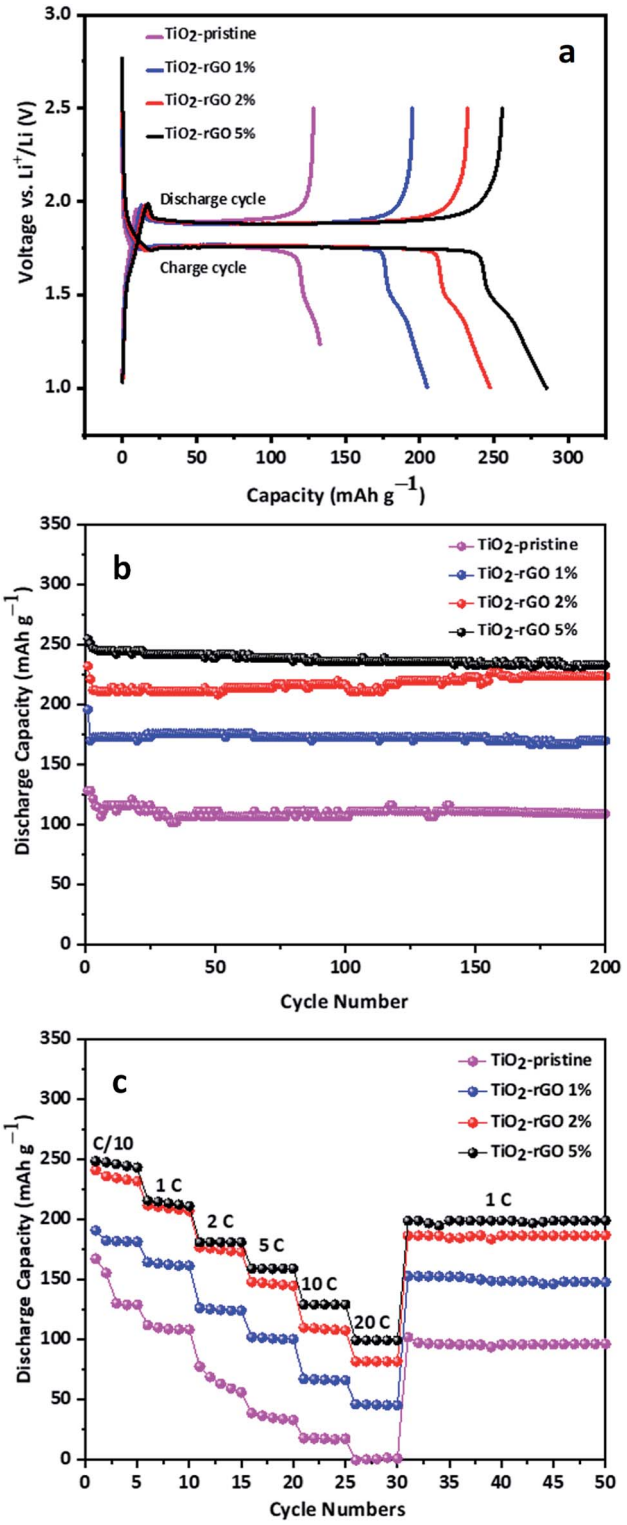

Fig. 4 Electrochemical characteristics of TiO_2–pristine, TiO_2–rGO 1%, TiO_2–rGO 2%, TiO_2–rGO 5%: (a) voltage profiles for the first cycle, (b) cycle performances at a rate of 0.2C (c) rate capability performance at a range of current densities.

performance, all the cells were subjected to current densities ranging from 0.1 to 20C with identical discharge and charge current density and five charge/discharge cycles at each current density. The results presented in Fig. 4c show that at a current density of 0.1C, both TiO_2–rGO 5% and TiO_2–rGO 2% possess a noticeably higher capacity than TiO_2–rGO 1%, which is also higher than TiO_2–pristine. As the C-rate was increased from 1 to 20C, the capacities of TiO_2–pristine sample declined from 167 mA h g^{-1} to almost zero. At up to 2C the capacities for TiO_2–rGO 5% and TiO_2–rGO 2% remained comparable, but at 5C and above the TiO_2–rGO 5% anode showed the highest capacity, achieving 100 mA h g^{-1} or above at current densities as high as 20C. At 20C, the TiO_2–rGO 5% anode retained 40% of the capacity recorded at 0.1C. When returned to 1C after cycling at 20C, the samples retained their capacities nicely and remained stable for the next 20 cycles. TiO_2-based anodes have been studies previously, including at even higher C-rates; however, the achievable discharge capacity remained in the range of *ca.* 100 mA h g^{-1}.[42] Stable discharge capacities of *ca.* 161 mA h g^{-1}

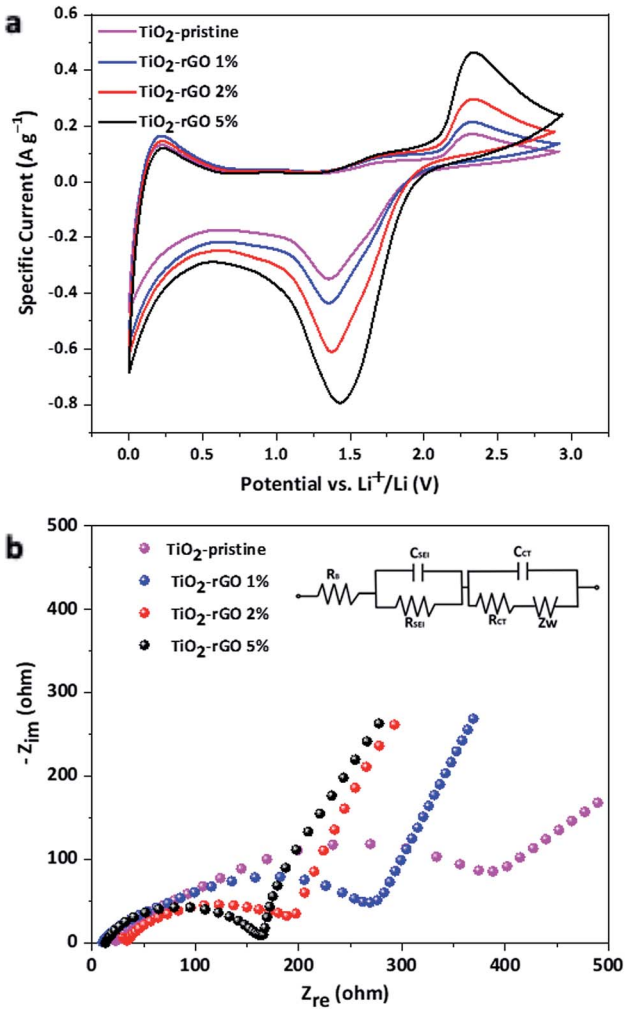

Fig. 5 (a) Representative cyclic voltammograms of TiO_2–pristine, TiO_2–rGO 1%, TiO_2–rGO 2%, TiO_2–rGO 5% at a scan rate of 0.5 mV s^{-1} between 0 V and 3 V; (b) EIS Nyquist plots of the same samples, along with the equivalent circuit (R_B is the bulk resistance, R_{SEI} and C_{SEI} are the resistance and capacitance of the solid electrolyte interface, R_{CT} and C_{CT} are the charge transfer resistance and capacitance, and Z_W is the Warburg impedance).

at 5C, *ca.* 129 mA h g^{-1} at 10C, and *ca.* 100 mA h g^{-1} at 20C, were obtained for the TiO_2–rGO 5% anode. These capacities demonstrate that the rGO contributed significantly to enhanced electrochemical performance in comparison to other recent studies of TiO_2 based anodes.[43]

Cyclic voltammetry (CV) is a useful electrochemical technique to evaluate redox potentials of reversible systems. CV results for the TiO_2 nanocomposite samples were recorded using a potential window 0.0 to 3.0 V *vs.* Li^+/Li are shown in Fig. 5a. The CV results show no significant change in the redox potentials, but differences in the magnitude of the cathodic and anodic peak currents were observed. A higher amplitude in the cathodic and anodic peak currents (at around 1.45 V and 1.5 V respectively) was observed for TiO_2–rGO 5%, indicating higher redox activity in terms of current for this sample. It is evident from the results that beside the characteristic pair of current peaks from the anatase TiO_2, broad peaks were also recorded in the lower voltage range around 0.1 V. These cathodic and anodic peaks can be attributed to additional electrochemical processes including formation of an SEI layer taking place due to the presence of rGO and Super P carbon black in the electrode. However, further studies are required to understand the impact of carbon in the TiO_2 electrodes.

Electrochemical impedance spectroscopy (EIS) was conducted to investigate the electrode resistance and active material-current collector interfacial resistance. The results of EIS study is illustrated using the Nyquist spectra shown in Fig. 5b. The shape of the impedance arc (depressed or distinct) depends on the total resistance offered by the cell. In the case of the four different samples the contact resistance was strongly dependent on the amount of GO present in the composite due to differences in the electron mobility in the nanocomposites. For the TiO_2–pristine, the poor electrical contact hindered the electron flow from the Cu current collector to the active materials, consistent with previous studies.[41,44,45] The high contact resistance for the TiO_2–pristine led to a large overall resistance of ~387 Ω, calculated from the *x*-intercept of impedance arc. The total resistance for TiO_2–rGO 5% was ~164 Ω, which is about 60% decrease in overall resistance of the pristine cell. From the EIS results it is evident that the TiO_2–rGO 2% and 5% nanocomposite anodes have low surface resistance, enabling the high capacity and rate capability of the half-cell using these materials.

Conclusions

In this study, rGO was investigated as an additive to enhance the conductivity of TiO_2 anodes. TiO_2–rGO nanocomposites were synthesized by a simple and rapid *in situ* method. The experimental results demonstrated that TiO_2 nanoparticles homogenously dispersed on rGO nanosheets could be obtained. The electrochemical results demonstrate that high rate capability and cycle stability could be achieved with the developed TiO_2–rGO electrode. The well-integrated rGO nano-filler enhanced the electrode conductivity enabling the increased rate capability of the TiO_2-electrodes. The as-prepared TiO_2–rGO nanocomposite showed potential for use as a viable anode material in advanced Li-ion battery applications which require high power.

Conflicts of interest

There are no conflicts to declare.

Acknowledgements

The authors acknowledge the financial support from Natural Sciences and Engineering Research Council of Canada (NSERC). This work contributes to the research performed at CELEST (Center for Electrochemical Energy Storage Ulm-Karlsruhe).

References

1 M. Armand, Nature Lithium Battery, *Nature*, 2001, **414**, 359–367.
2 E. Ferg, R. J. Gummow, A. D. Kock and M. M. Thackeray, Spinel anodes for lithium-ion batteries, *J. Electrochem. Soc.*, 1994, **141**(11), L147–L150.
3 A. R. Armstrong, G. Armstrong, J. Canales, R. García and P. G. Bruce, Lithium-ion intercalation into TiO_2-B nanowires, *Adv. Mater.*, 2005, **17**(7), 862–865.
4 C. Arrouvel, S. C. Parker and M. S. Islam, Lithium Insertion and Transport in the TiO_2—B Anode Material: A Computational Study, *Chem. Mater.*, 2009, **21**(20), 4778–4783.
5 M. B. Vazquez-Santos, P. Tartaj, E. Morales and J. M. Amarilla, TiO_2 Nanostructures as Anode Materials for Li/Na-Ion Batteries, *Chem. Rec.*, 2018, **18**(7), 1178–1191.
6 M. Madian, A. Eychmüller and L. Giebeler, Current advances in TiO_2-based nanostructure electrodes for high performance lithium ion batteries, *Batteries*, 2018, **4**(1), 7.
7 P. Li, P. Li, X. Guo, S. Wang, R. Zang, X. Li, Z. Man, S. Liu, Y. Wu and G. Wang, Two-dimensional Sb@TiO_{2-x} nanoplates as a high-performance anode material for sodium-ion batteries, *J. Mater. Chem. A*, 2019, **7**(6), 2553–2559.
8 D. Deng, M. G. Kim, J. Y. Lee and J. Cho, Green energy storage materials: nanostructured TiO_2 and Sn-based anodes for lithium-ion batteries, *Energy Environ. Sci.*, 2009, **2**(8), 818–837.
9 J. Zhang, X. Yan, J. Zhang, W. Cai, Z. Wu and Z. Zhang, Preparation and electrochemical performance of TiO_2/C composite nanotubes as anode materials of lithium-ion batteries, *J. Power Sources*, 2012, **198**, 223–228.
10 J. Y. Cheong, C. Kim, J. W. Jung, T. G. Yun, D. Y. Youn, S. H. Cho, K. R. Yoon, H. Y. Jang, S. W. Song and I. D. Kim, Incorporation of amorphous TiO_2 into one-dimensional SnO_2 nanostructures as superior anodes for lithium-ion batteries, *J. Power Sources*, 2018, **400**, 485–492.
11 T. Song and U. Paik, TiO_2 as an active or supplemental material for lithium batteries, *J. Mater. Chem. A*, 2015, **4**(1), 14–31.

12 Y. Liu, J. Liu, D. Bin, M. Hou, A. G. Tamirat, Y. Wang and Y. Xia, Ultrasmall TiO_2-Coated Reduced Graphene Oxide Composite as a High-Rate and Long-Cycle-Life Anode Material for Sodium-Ion Batteries, *ACS Appl. Mater. Interfaces*, 2018, **10**(17), 14818–14826.

13 S. Nagpure, Q. Zhang, M. A. Khan, S. Z. Islam, J. Xu, J. Strzalka, Y. T. Cheng, B. L. Knutson and S. E. Rankin, Layer-by-Layer Synthesis of Thick Mesoporous TiO_2 Films with Vertically Oriented Accessible Nanopores and Their Application for Lithium-Ion Battery Negative Electrodes, *Adv. Funct. Mater.*, 2018, **28**(37), 1–10.

14 H. Han, T. Song, J. Y. Bae, L. F. Nazar, H. Kim and U. Paik, Nitridated TiO_2 hollow nanofibers as an anode material for high power lithium ion batteries, *Energy Environ. Sci.*, 2011, **4**(11), 4532–4536.

15 K. Hwang, H. Sohn and S. Yoon, Mesostructured niobium-doped titanium oxide-carbon (Nb-TiO_2-C) composite as an anode for high-performance lithium-ion batteries, *J. Power Sources*, 2018, **378**, 225–234.

16 W. Song, J. Chen, X. Ji, X. Zhang, F. Xie and D. J. Riley, Dandelion-shaped TiO_2/multi-layer graphene composed of TiO_2(B) fibrils and anatase TiO_2 pappi utilizing triphase boundaries for lithium storage, *J. Mater. Chem. A*, 2016, **4**(22), 8762–8768.

17 W. Zheng, Z. Yan, Y. Dai, N. Du, X. Jiang, H. Dai, X. Li and G. He, Interpenetrated Networks between Graphitic Carbon Infilling and Ultrafine TiO_2 Nanocrystals with Patterned Macroporous Structure for High-Performance Lithium Ion Batteries, *ACS Appl. Mater. Interfaces*, 2017, **9**(24), 20491–20500.

18 I. Moriguchi, R. Hidaka, H. Yamada, T. Kudo, H. Murakami and N. Nakashima, A mesoporous nanocomposite of TiO_2 and carbon nanotubes as a high-rate Li-intercalation electrode material, *Adv. Mater.*, 2006, **18**(1), 69–73.

19 S. Pervez, D. Kim, C. H. Doh, U. Farooq, A. Yaqub, J. H. Choi, Y. J. Lee and M. Saleem, High areal capacity for battery anode using rapidly growing self-ordered TiO_2 nanotubes with a high aspect ratio, *Mater. Lett.*, 2014, **137**, 347–350.

20 Z. Li, H. Zhao, P. Lv, Z. Zhang, Y. Zhang, Z. Du, Y. Teng, L. Zhao and Z. Zhu, Watermelon-Like Structured SiO_x–TiO_2@C Nanocomposite as a High-Performance Lithium-Ion Battery Anode, *Adv. Funct. Mater.*, 2018, **28**(31), 1–11.

21 V. Aravindan, Y. S. Lee, R. Yazami and S. Madhavi, TiO_2 polymorphs in "rocking-chair" Li-ion batteries, *Mater. Today*, 2015, **18**(6), 345–351.

22 X. Gao, X. Sun, Z. Jiang, Q. Wang, N. Gao, H. Li, H. Zhang, K. Yu and C. Su, Introducing nanodiamond into TiO_2-based anode for improving the performance of lithium-ion batteries, *New J. Chem.*, 2019, **43**(9), 3707–3712.

23 S. Bashir, P. Hanumandla, H. Y. Huang and J. L. Liu, Nanostructured materials for advanced energy conversion and storage devices: safety implications at end-of-life disposal. Nanostructured Mater. Next-Generation Energy Storage Convers, *Fuel Cells*, 2018, **4**, 517–542.

24 S. Jiang, R. Wang, M. Pang, H. Wang, S. Zeng, X. Yue, L. Ni, Y. Yu, J. Dai, S. Qiu and Z. Zhang, Assembling porous carbon-coated TiO_2(B)/anatase nanosheets on reduced graphene oxide for high performance lithium-ion batteries, *Electrochim. Acta*, 2015, **182**, 406–415.

25 A. Mondal, S. Maiti, K. Singha, S. Mahanty and A. B. Panda, TiO_2-rGO nanocomposite hollow spheres: large scale synthesis and application as an efficient anode material for lithium-ion batteries, *J. Mater. Chem. A*, 2017, **5**(45), 23853–23862.

26 B. Zhang, Y. Yu, Y. Liu, Z. D. Huang, Y. B. He and J. K. Kim, Percolation threshold of graphene nanosheets as conductive additives in $Li_4Ti_5O_{12}$ anodes of Li-ion batteries, *Nanoscale*, 2013, **5**(5), 2100–2106.

27 E. Lim, H. Shim, S. Fleischmann and V. Presser, Fast and stable lithium-ion storage kinetics of anatase titanium dioxide/carbon onion hybrid electrodes, *J. Mater. Chem. A*, 2018, **6**(20), 9480–9488.

28 T. Kogure and T. Umezawa, Formation of TiO_2 (B) Nanocrystallites in Sol-Gel-Derived SiO_2-TiO_2 Film, *J. Am. Ceram. Soc.*, 1999, **50**, 3248–3250.

29 M. Pfanzelt, Development of TiO_2 Rutile as Negative Electrode Material for Lithium Ion Batteries, PhD Dissertation, Ulm University, 2012.

30 H. Han, T. Song, E. K. Lee, A. Devadoss, Y. Jeon, J. Ha, Y. C. Chung, Y. M. Choi, Y. G. Jung and U. Paik, Dominant factors governing the rate capability of a TiO_2 nanotube anode for high power lithium ion batteries, *ACS Nano*, 2012, **6**(9), 8308–8315.

31 D. Dambournet, I. Belharouak and K. Amine, Tailored preparation methods of TiO_2 anatase, rutile, brookite: mechanism of formation and electrochemical properties, *Chem. Mater.*, 2010, **22**(3), 1173–1179.

32 V. Mathew, J. Gim, M. H. Alfaruqi, S. Kim, J. Song, J. P. Baboo, S. Kim, S. Park, D. Kim and J. Kim, A porous TiO_2 electrode prepared by an energy efficient pyro-synthesis for advanced lithium-ion batteries, *J. Electrochem. Soc.*, 2015, **162**(7), A1220–A1226.

33 X. Xin, X. Zhou, J. Wu, X. Yao and Z. Liu, Scalable synthesis of TiO_2/graphene nanostructured composite with high-rate performance for lithium ion batteries, *ACS Nano*, 2012, **6**(12), 11035–11043.

34 W. S. Hummers and R. E. Offeman, Preparation of Graphitic Oxide, *J. Am. Chem. Soc.*, 1958, **80**(6), 1339.

35 V. Augustyn, J. Come, M. A. Lowe, J. W. Kim, P. L. Taberna, S. H. Tolbert, H. D. Abruña, P. Simon and B. Dunn, High-rate electrochemical energy storage through Li^+ intercalation pseudocapacitance, *Nat. Mater.*, 2013, **12**(6), 518–522.

36 H. E. Wang, H. Cheng, C. Liu, X. Chen, Q. Jiang, Z. Lu, Y. Y. Li, C. Y. Chung, W. Zhang, J. A. Zapien, L. Martinu and I. Bello, Facile synthesis and electrochemical characterization of porous and dense TiO_2 nanospheres for lithium-ion battery applications, *J. Power Sources*, 2011, **196**(15), 6394–6399.

37 M. C. Yang, Y. Y. Lee, B. Xu, K. Powers and Y. S. Meng, TiO_2 flakes as anode materials for Li-ion-batteries, *J. Power Sources*, 2012, **207**, 166–172.

38 J. Y. Hwang, H. L. Du, B. N. Yun, M. G. Jeong, J. S. Kim, H. Kim, H. G. Jung and Y. K. Sun, Carbon-Free TiO_2

Microspheres as Anode Materials for Sodium Ion Batteries, *ACS Energy Lett.*, 2019, **4**(2), 494–501.

39 U. Lafont, D. Carta, G. Mountjoy, A. V. Chadwick and E. M. Kelder, In situ structural changes upon electrochemical lithium insertion in nanosized anatase TiO_2, *J. Phys. Chem. C*, 2010, **114**(2), 1372–1378.

40 M. G. Choi, Y. G. Lee, S. W. Song and K. M. Kim, Anode properties of titanium oxide nanotube and graphite composites for lithium-ion batteries, *J. Power Sources*, 2010, **195**(24), 8289–8296.

41 M. Mao, F. Yan, C. Cui, J. Ma, M. Zhang, T. Wang and C. Wang, Pipe-wire TiO_2-Sn@carbon nanofibers paper anodes for lithium and sodium ion batteries, *Nano Lett.*, 2017, **17**(6), 3830–3836.

42 J. H. Jeong, M. S. Kim, Y. H. Kim, K. C. Roh and K. B. Kim, High-rate $Li_4Ti_5O_{12}$/N-doped reduced graphene oxide composite using cyanamide both as nanospacer and a nitrogen doping source, *J. Power Sources*, 2016, **336**, 376–384.

43 D. P. Opra, S. V. Gnedenkov and S. L. Sinebryukhov, Recent efforts in design of TiO_2(B) anodes for high-rate lithium-ion batteries: a review, *J. Power Sources*, 2019, **442**, 227225.

44 M. Wagemaker, A. P. M. Kentjens and F. M. Mulder, Equilibrium lithium transport between nanocrystalline phases in intercalated TiO_2 anatase, *Nature*, 2002, **418**(6896), 397–399.

45 Y. Liu, Y. K. Tzeng, D. Lin, A. Pei, H. Lu, N. A. Melosh, Z. X. Shen, S. Chu and Y. Cui, An Ultrastrong Double-Layer Nanodiamond Interface for Stable Lithium Metal Anodes, *Joule*, 2018, **2**(8), 1595–1609.